Moist processes during MJO events as diagnosed from water isotopic measurements from the IASI satellite

Obbe A. Tuinenburg, Camille Risi, Jean Lionel Lacour, Matthias Schneider, Andreas Wiegele, John Worden, N. Kurita, Jean-Philippe Duvel, Nicholas Deutscher, Sandrine Bony, et al.

AGU PUBLICATIONS

JGR

Journal of Geophysical Research: Atmospheres

RESEARCH ARTICLE
10.1002/2015JD023461

Key Points:
- Variability between MJO events 5–10 days after the event
- More inter-MJO event variability over maritime continent than Indian Ocean
- Water isotopes are useful for GCM process validation

Correspondence to:
O. A. Tuinenburg,
Obbe.Tuinenburg@lmd.jussieu.fr

Citation:
Tuinenburg, O. A., et al. (2015), Moist processes during MJO events as diagnosed from water isotopic measurements from the IASI satellite, *J. Geophys. Res. Atmos.*, *120*, 10,619–10,636, doi:10.1002/2015JD023461.

Received 8 APR 2015
Accepted 17 SEP 2015
Accepted article online 22 SEP 2015
Published online 20 OCT 2015

Moist processes during MJO events as diagnosed from water isotopic measurements from the IASI satellite

O. A. Tuinenburg[1], C. Risi[1], J. L. Lacour[2], M. Schneider[3], A. Wiegele[3], J. Worden[4], N. Kurita[5], J. P. Duvel[6], N. Deutscher[7], S. Bony[1], P. F. Coheur[2], and C. Clerbaux[2,8]

[1]Laboratoire de Météorologie Dynamique, IPSL, UPMC, CNRS, Paris, France, [2]Spectroscopie de l'Atmosphère, Service de Chimie Quantique et Photophysique, Université Libre de Bruxelles, Brussels, Belgium, [3]Karlsruhe Institute of Technology, Karlsruhe, Germany, [4]NASA JPL, Pasadena, California, USA, [5]Graduate School of Environmental Studies, Nagoya University, Nagoya, Japan, [6]Laboratoire de Meteorologie Dynamique, CNRS, ENS, Paris, France, [7]Centre for Atmospheric Chemistry, University of Wollongong, Wollongong, Australia, [8]UPMC Pierre et Marie Curie Universite, Universite Versailles St-Quentin, CNRS/INSU, LATMOS-IPSL Paris, France

Abstract This study aims to investigate some characteristics of the moist processes of the Madden-Julian oscillation (MJO), by making use of joint HDO (or δD) and H_2O vapor measurements. The MJO is the main intraseasonal mode of the tropical climate but is hard to properly simulate in global atmospheric models. The joint use of δD-H_2O diagnostics yields additional information compared to sole humidity measurements. We use midtropospheric Infrared Atmospheric Sounding Interferometer (IASI) satellite δD and H_2O measurements to determine the mean MJO humidity and δD evolution. Moreover, by making use of high temporal resolution data, we determine the variability in this evolution during about eight MJO events from 2010 to 2012 (including those monitored during the DYNAMO (the Dynamics of the MJO), CINDY (Cooperative Indian Ocean Experiment in Y2011) campaign). These data have a higher spatiotemporal coverage than previous δD measurements, enabling the sampling of individual MJO events. IASI measurements over the Indian Ocean confirm earlier findings that the moistening before the precipitation peak of an MJO event is due to water vapor slightly enriched in HDO. There is then a HDO depletion around the precipitation peak that also corresponds to the moister environment. Most interevent variability determined in the current study occurs 5 to 10 days after the MJO event. In 75% of the events, humidity decreases while the atmosphere remains depleted. In a quarter of the events, humidity increases simultaneously with an increase in δD. After this, the advection of relatively dry and enriched air brings back the state to the mean. Over the maritime continent, δD-H_2O cycles are more variable on time scales shorter than the MJO and the interevent variability is larger than over the Indian Ocean. The sequence of moistening and drying processes as revealed by the q-δD cycles can be used as a benchmark to evaluate the representation of moist processes in models. This is done here by comparing observations to simulations of the isotope enabled LMDZ (Laboratoire de Météorologie Dynamique Zoom) global climate model nudged with reanalysis wind fields. These simulations also give information to investigate possible physical origins of the observed q-δD cycles.

1. Introduction

The Madden-Julian oscillation (MJO) [*Madden and Julian*, 1972] is a phenomenon in which tropical convective activity recurs in active and inactive phases with a cycle of between 20 and 90 days. It is an important mode of variability in the tropics, where it affects precipitation directly, as well as in other areas around the world where it modifies weather patterns indirectly [*Zhang*, 2013].

Canonical Northern Hemisphere winter MJO events start as convective anomalies off the eastern coast of Africa and travel eastward across the Indian Ocean, over the maritime continent, and into the Pacific. Although the convective anomalies decay over cooler sea surfaces, the wind patterns associated with the MJO may go around the globe [*Matthews*, 2000]. Figure 1 shows a schematic of the midtropospheric MJO moist processes and typical wind patterns for a composite of MJO events with the peak of convective activity at 90°E.

Current atmospheric models have trouble representing the MJO variability as observed [*Randall*, 2013]. The MJO is an oscillation that involves interaction between the sea surface, evaporation, convective organization, advection of moisture, and radiation [*Woolnough et al.*, 2007; *Zhang*, 2005; *Randall*, 2013; *Zhang et al.*, 2013; *Sobel and Maloney*, 2013; *Sobel et al.*, 2014; Yokoi and Sobel, submitted to *Journal of the Meteorological Society*

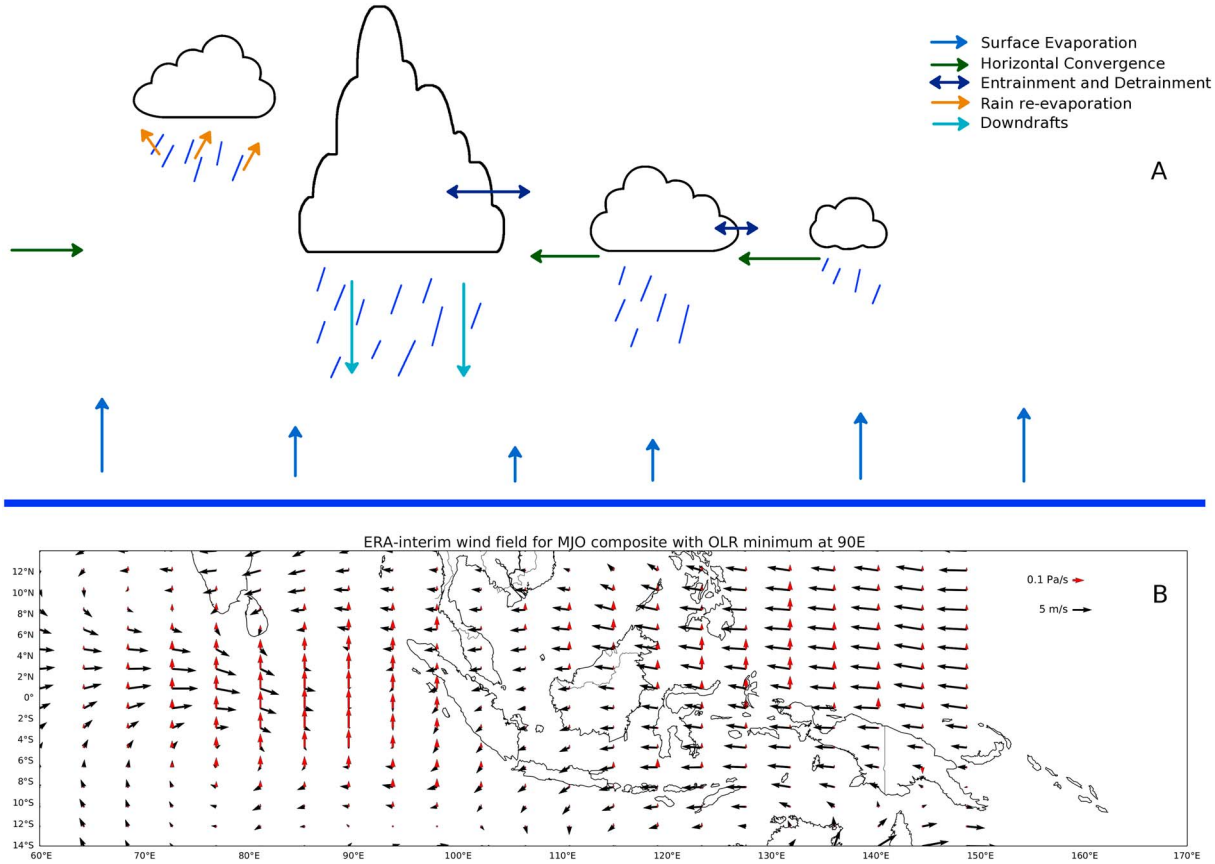

Figure 1. Composite of MJO events (2010–2012) with a peak of convective activity at 90°E. (a) MJO cloud schematic, with moistening and drying processes based on *Lau and Peng* [1987], *Flatau et al.* [1997], *Kiladis and Weickmann* [1992], *Benedict and Randall* [2007], *Berkelhammer et al.* [2012], and *Kurita et al.* [2011]. (b) ERA-interim wind fields at 500 hPa (horizontal winds in black, vertical in red).

of Japan, 2015]. It involves the interaction between different processes, such as humidity, shallow convection, deep convection, large-scale dynamics, high stratiform clouds, and cloud-radiative interaction. The simulation of the MJO is sensitive to the representation of convection in the model [*Hung et al.*, 2013; *Kim et al.*, 2009, 2012; *Thayer-Calder and Randall*, 2009; *Maloney and Hartmann*, 2001]. Some studies suggest that atmospheric models do not simulate the MJO well because the moisture buildup in the atmosphere is insufficient [*Randall*, 2013]. Before the very high humidities that occur in nature during the peak of MJO events, precipitation occurs in the models, which dries the atmosphere. A better understanding of these convective processes during the different stages of the MJO can improve the simulation of the MJO in atmospheric models.

This study uses measurements of specific humidity and stable water isotopes (HDO) at 500 hPa to determine the moist processes during the MJO. A HDO molecule is slightly heavier than a normal water molecule. Consequently, the HDO molecules have a preference to be present in the phase with a lower energy state. So, as a result of evaporation and condensation, the ratio of heavier molecules to normal water molecules will be higher in the liquid phase than in the gas phase. Due to this fractionation, measurements of stable water isotopes can be used to study moist processes. For example, in two air masses with the same humidity and different precipitation rates, the air mass with the lower precipitation rate is expected to have a higher reevaporation of falling droplets. This reevaporation leads to lower HDO concentrations compared to the air mass with the higher-precipitation rate.

We use the δ notation to describe the (relative) concentration of HDO. δD is a measure of the relative abundance of HDO

$$\delta\mathrm{D} = 1000\left(\frac{R}{R_{\mathrm{VSMOW}}} - 1\right) \tag{1}$$

in which R is the ratio of HDO to normal water (H_2O) and R_{VSMOW} is the reference value (Vienna Standard Mean Ocean Water) for this ratio (155.76 ppm). δD ranges from −1000‰ (strong depletion, no HDO molecules

present), 0‰ (same ratio of heavier to normal isotope as standard seawater) to ∞ (theoretically, only heavier molecule present). Typical values for the tropical midtroposphere are −300 to −150‰.

The measurements of q and δD are jointly analyzed here, as these measurements are correlated. Therefore, it is the change in δD relative to a change in q that provides process information on air mass processes and origin [*Noone*, 2012], potentially distinguishing between Rayleigh distillation, surface mixing, reevaporation, and advection [*Noone*, 2012; *Worden et al.*, 2006; *Galewsky and Hurley*, 2010].

Berkelhammer et al. [2012] used stable water isotopes from the Tropospheric Emission Spectrometer (TES) satellite [*Worden et al.*, 2012] to determine the moisture sources during the MJO. By analyzing a composite of MJO events, they determined evaporative moisture to be the dominant moisture source during the early onset of the MJO. During subsequent convective development, this signal was less prevalent, but it emerged again during the peak of the MJO event. As the temporal coverage of their data was more limited than in the current study, *Berkelhammer et al.* [2012] could only analyze a composite of MJO events and found a dominant "anticlockwise" q-δD cycle, in which moistening was followed by enrichment, drying, and, finally, depletion (see section 2.5).

This paper shows how stable water isotopes can be used as process diagnostics for climate models. First, it presents the Infrared Atmospheric Sounding Interferometer (IASI) q-δD data set for the MJO domain and compares the IASI data to several alternative data sets with different spatiotemporal sampling or instrumental sensitivity. The IASI data set has a higher temporal coverage than previous isotopic data sets used to assess the MJO moisture sources. Due to its sampling characteristics (a measurement almost everywhere twice daily), IASI can be used to determine the q-δD signal of individual MJO events, whereas previous studies could only make composites over several MJO events. However, only cloud-free measurements can be exploited for δD. The IASI instrument sensitivity is maximal at 500 hPa, whereas most moisture variability occurs lower in the troposphere.

Second, the composite mean IASI q-δD MJO phasing is determined, and these vary significantly in space. Over the Indian Ocean, the q-δD phasing is significantly different than over the maritime continent. Moreover, the spatial variability in the MJO signal are compared to the variability between the MJO events at a given location. Over the Indian Ocean, there is little variability among the different MJO events. However, over the maritime continent, the variability in q-δD phasing between the MJO events is large.

Third, a physical interpretation of the MJO q-δD phasing is made based on an isotope-enabled atmospheric model. The relative importance of the condensation and mixing processes and the advection of moisture is determined during all phases of the MJO cycle. Comparison of model and observations suggests that the main source of variability between events over the Indian Ocean lies in the relative fraction of convection and large-scale condensation. Over the maritime continent, the variability between the events is probably due to the importance of synoptic events and the interaction with the land masses.

This paper is structured as follows. Section 2 describes and compares the data sets and models used. Section 3 describes the mean MJO cycles, its spatial and interevent variability, and the proposed physical explanation for these observations. Sections 4 and 5 present the discussion and conclusions.

2. Methods

2.1. Identification of MJO Events

MJO events are determined using the NOAA outgoing longwave radiation (OLR) time series [*Liebmann and Smith*, 1996]. The variability with frequencies larger than 90 days and smaller than 30 days is filtered to get the MJO time series (as in *Berkelhammer et al.* [2012]). The center of an event is diagnosed when there is a local filtered OLR minimum with a value smaller than the 10th percentile in this filtered OLR time series of a given large region. Sensitivity tests showed that the number of events and dates of the OLR minimum are not very sensitive to this percentile value. This procedure may have spuriously identified some events as MJO events, while in reality they were caused by other tropical waves. Although a lot of time has been spent to quality control the process by inspecting the OLR time series, the anomalous q-δD phasing of some diagnosed events could be due to an incorrect diagnosis of MJO events.

The precipitation maximum is detected using Tropical Rainfall Measurement Mission (TRMM) data [*Huffman et al.*, 2007] in a large interval of 20 days centered on the date of the OLR minimum.

2.2. IASI Data Set

This study mainly uses δD estimates derived from IASI measurements. The IASI instrument flying on board MetOp satellites from European Organisation for the Exploitation of Meteorological Satellites (EUMETSAT) measures thermal infrared radiation emitted by the Earth with overpasses twice daily at around 9.30 A.M. and 9.30 P.M. local solar time [*Clerbaux et al.*, 2009]. The data used in this study originate from the first satellite (of three) put in orbit during the IASI mission. It has been retrieved in the Indian Ocean and maritime continent (65–155°E, 15°S–10°N).

Retrieving concentration profiles of atmospheric constituents from infrared measurements constitutes an inverse problem and necessitates an inversion procedure to be performed. Solutions of the inversion contain a certain part of a priori information. The quantity of that information depends on the regularization procedure and can differ from one inversion scheme to another. Here we used two different retrieval products developed, respectively, at Université Libre de Bruxelles (ULB) and at Karlsruhe Institute for Technology (KIT). These two different products and the recent efforts to characterize them are briefly presented here.

2.2.1. IASI ULB Retrieval

At ULB, the retrieval procedure used a relatively short range of IASI spectra, only the first 10 km of the atmosphere is adjusted during the retrieval, temperature profiles from EUMETSAT are used, and cloud contaminated spectra are avoided [*Lacour et al.*, 2012]. The profiles have been recently cross validated against TES δD profiles and three ground-based Fourier transform infrareds (FTIRs, data generated in the context of the multiplatform remote sensing of isotopologues for investigating the cycle of atmospheric water (MUSICA) project) with an error of about 38‰ in the free troposphere on a single measurement basis [*Lacour et al.*, 2015]. ULB retrieval products have been used to assess q-δD phasing over the whole period of this study (March 2010 to March 2012).

2.2.2. IASI KIT Retrieval

The IASI KIT (Karlsruhe Institute of Technology) water vapor isotopologue retrieval has been developed in the framework of the project MUSICA (multiplatform remote sensing of isotopologues for investigating the cycle of atmospheric water, http://www.imk-asf.kit.edu/english/musica.php), which integrates space-based remote sensing, ground-based remote sensing, and well calibrated in situ experiments.

The KIT retrieval uses a broad spectral window (1190–1400 cm^{-1}), a fine gridded atmospheric model, and works as a simultaneous optimal estimation of H_2O and δD as well as of the interfering gases (CH_4, N_2O, CO_2, and HNO_3) and temperature [*Schneider and Hase*, 2011]. The isotopologue products have been validated with respect to the MUSICA ground-based FTIR remote sensing data (using spectra measured with the Network for the Detection of Atmospheric Composition Change) and to the well-calibrated MUSICA in situ reference data (aircraft based and continuous surface based) [*Schneider et al.*, 2015; *Dyroff et al.*, 2015]. The MUSICA in situ aircraft reference data (0–7 km) allow a first adequate bias correction, or calibration, of the retrieval results [*Schneider et al.*, 2015; *Dyroff et al.*, 2015]. The overall uncertainty for an individual observation has been estimated to about 10% and 35‰ for q and for δD, respectively, [*Wiegele et al.*, 2014].

During MUSICA, a retrieval postprocessing has been developed [*Schneider et al.*, 2012]. It assures that the provided q and δD products represent almost the same water mass, i.e., it is the q-δD pair that is optimally estimated (it is not an individual optimal estimation of q and δD). This strongly facilitates a correct interpretation of the q-δD plots.

2.2.3. Uncertainties Related to IASI Data

The majority of this work is based on satellite data. For the IASI satellite and the retrieval algorithms used, the instrument sensitivity is maximal at 500 hPa, and the estimated total measurement error is about 38‰ [*Lacour et al.*, 2012] per measurement at 500 hPa. This is about the same magnitude of the typical δD variability over the Indian Ocean. If the measurements are assumed to be independent, a sample mean based upon n measurements has an error of $38‰/\sqrt{(n)}$. Typically, there are 60 samples per day per LMDZ (see section 2.4) grid cell. This decreases the δD error per grid cell to about 4‰ (it is about 6‰ during the MJO peak, when the sampling is lower due to cloud cover). As almost all MJO events over the Indian Ocean have similar q-δD phasing, this phasing seems robust. Over the maritime continent, the MJO δD signal is smaller. Moreover, over the maritime continent, the δD variability across events is larger than the measurement error, while the δD variability across events is smaller than the measurement error over the Indian Ocean.

Moreover, there are some potential uncertainties associated with the sampling of the IASI satellite. The retrieval algorithm can only be applied over cloud-free areas. Therefore, the measurements are representative

for the environments around the clouds. This means that the δD variability will be underestimated compared to in situ measurements, as these take into account the areas under and in clouds where moisture is likely to be more depleted due to the condensation and reevaporation processes there. On the other hand, the cloud-free areas are more likely to be subsiding air, which is more likely to be depleted. Furthermore, the number of IASI measurements per LMDZ grid cell (3.75×2.5°) decreases from around 90 during cloud-free, convectively suppressed conditions to 25 during peak of the MJO event, as a larger fraction is covered with clouds. To quantify the effect of sample number on the δD evolution during the MJO, the correlation between the LMDZ model and IASI δD, conditional on the number of IASI measurements per grid cell, was determined. For large number of measurements (60–90 per LMDZ grid cell), the correlation is about 0.4–0.45; between 20 and 60 measurements, the correlation is about 0.35; while for less than 20 measurements per grid cell, the correlation sharply drops off to below 0.2. The minimum of 25 observations during the MJO peak is still above the correlation drop off, which gives some confidence that the δD phasing is reasonable.

The IASI satellite has two overpasses per day, and this study aggregates measurements from both overpasses to a daily value. During periods with a lot of convection (the peak of the MJO event), there is more data from the morning overpasses, as the chance of clouds is higher during the afternoon. We tested the effect of this preferential morning sampling on the MJO q-δD signals and found similar signals from morning and evening overpasses. The morning overpasses over the Indian ocean are on average about 0.04 g/kg drier, and δD is 2‰ more depleted than the evening overpasses. Over the maritime continent, the morning overpasses are 0.06 g/kg moister and 4.5‰ more enriched than the evening overpasses. These differences are a lot smaller than the typical MJO variability for q and δD.

2.3. Additional Isotopic Data

We use several alternative q-δD data sets to compare with IASI:

1. The q-δD product (at 600 hPa) from the TES instrument [*Worden et al.*, 2012] provides δD retrieved profiles with up to two levels of information in the vertical (Version 5) but with lower spatiotemporal sampling than IASI.
2. The daily-average Total Carbon Column Observing Network (TCCON) data (version GGG2009) collected at the ARM site [*Deutscher et al.*, 2010] in Darwin, Australia, measures q and δD vertically integrated columns, and we calculate the column integrated δD, which is mainly sensitive to the variations of δD in the lower troposphere. A discussion of such δD product is given in *Rokotyan et al.* [2014]
3. The ship-based data measured during the CINDY-DYNAMO observation campaign [October 2011 to March 2012, *Zhang*, 2013] has a high temporal frequency (once every 30 min) and high precision but is surface based and is only representative of the location of the ship.

2.4. LMDZ Simulations

The q-δD signals of MJO events in this study are compared to the isotope enabled LMDZ general circulation model [*Risi et al.*, 2010] at its standard resolution (of 3.75×2.5°, with 39 vertical levels), nudged with ERA-interim reanalysis [*Dee et al.*, 2011] horizontal wind and forced with observed monthly sea surface temperatures. We use this nudged version to make the dynamics as close to reality as possible. Therefore, we can reliably assess the different processes during the MJO given a large-scale circulation that is as realistic as possible.

Biases in the LMDZ physics may limit its ability to reproduce the observed MJO cycle despite being nudged by reanalysis winds. Further, biases in the reanalysis forecast model could also lead to biases in the nudged LMDZ.

From the LMDZ model, the q and δD states are used at daily resolution. In the LMDZ model, the moisture balance (the δD balance is similar) is a sum of several processes, which are calculated independently

$$\frac{dq}{dt} = \frac{dq}{dt}_{\text{advection}} + \frac{dq}{dt}_{\text{lsce}} + \frac{dq}{dt}_{\text{con}} + \frac{dq}{dt}_{\text{bl}} \tag{2}$$

In this balance, the right-hand side gives the contributions of individual processes (hereafter tendencies) to the total moisture budget. The advection term represents the moisture convergence into the grid cell, the large-scale condensation and evaporation (lsce) are the condensation and evaporation that occur when the humidity in the grid box reaches some threshold and represents mostly stratiform cloud processes, the convection term (con) is due to the parametrization of convection at scales smaller than the grid cell, the boundary layer humidity term (bl) is due to surface evaporation, turbulent mixing, and the effect of organized

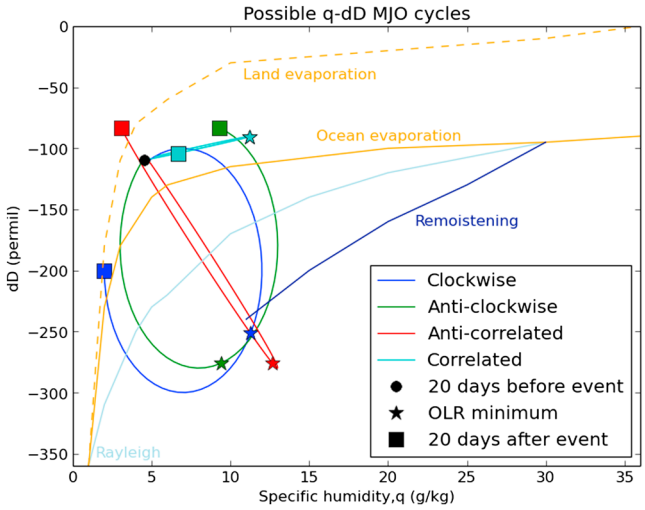

Figure 2. Examples of classification of MJO q-δD cycles into clockwise, anticlockwise, anticorrelated, and correlated cycles. All examples have the same initial q-δd value but different MJO progression. The dominant physical processes as determined by *Noone* [2012] are also shown.

convective structures within the boundary layer [*Rio et al.*, 2009]. The large-scale condensation and evaporation can also be activated when large-scale ascent occurs in the grid point, giving a sort of resolved convection (or "grid point storm").

2.5. Determination of Cycles

The q-δD data from the diagnosed MJO events are jointly analyzed and classified as either "clockwise," anticlockwise, "correlated," or anticorrelated, named after the temporal phasing in q-δD plots; examples of these cycles are shown in Figure 2. For this classification, both q and δD time series from 20 days prior to the OLR minimum to 20 days after the OLR minimum are taken as time series for the event. The mean is subtracted from these time series, after which a sinusoid (with period of 40 days) is fitted to each one separately. The classification is based on the phase difference between the fit to the q time series and the δD time series. An MJO event is classified correlated if the fits are in phase (phase difference < 5 days), anticorrelated if they are in opposite phase (phase difference 15–25 days), clockwise if the q fit lags a quarter phase (5–15 days), and anticlockwise if the q fit leads the δD fit a quarter phase (5–15 days). If the amplitude of the fit is smaller than 0.1 g/kg(q), or 5‰ (δD), an event is classified as having no variability in that variable. Events are also classified as having no variability if the mean absolute error of the fit is larger than the amplitude.

The processes affecting different MJO q-δD cycles can be determined using theoretical methods, such as by *Noone* [2012]. The mixing, condensation, and remoistening curves of *Noone* [2012] are shown in Figure 2. A clockwise cycle begins with dominant surface evaporation and Rayleigh distillation (in which isotopes are removed in thermodynamic and isotopic equilibrium), after which sub-Rayleigh processes (with depletion below the Rayleigh curve) [*Noone*, 2012] such as remoistening deplete the air of HDO, while humidity is high. After the OLR minimum, the air stays depleted while drying, due to strong condensation, finally the air mixes with advected, more enriched air and returns to the initial state. In an anticlockwise cycle, which was found to be the dominant MJO q-δD cycle by *Berkelhammer et al.* [2012], the strong depletion by condensation occurs before the OLR minimum. After the OLR minimum, the moisture enriches rapidly (for example, by mixing with surface air), while remaining relatively moist. In an anticorrelated cycle, moistening and depletion occur simultaneously before the OLR minimum, possibly due to co-occurrence of the previously mentioned processes. After the OLR minimum, enrichment and drying occur simultaneously, probably due to mixing with environmental air. For a correlated cycle, which is rare in the IASI data, a physical assessment is harder to make from the theoretical framework, as the dominant processes (surface mixing, Rayleigh distillation, and remoistening) depend in the initial state.

In addition to this physical interpretation based on *Noone* [2012], section 3.5 interprets the observed MJO q-δD cycles using the LMDZ global climate model (GCM) physics.

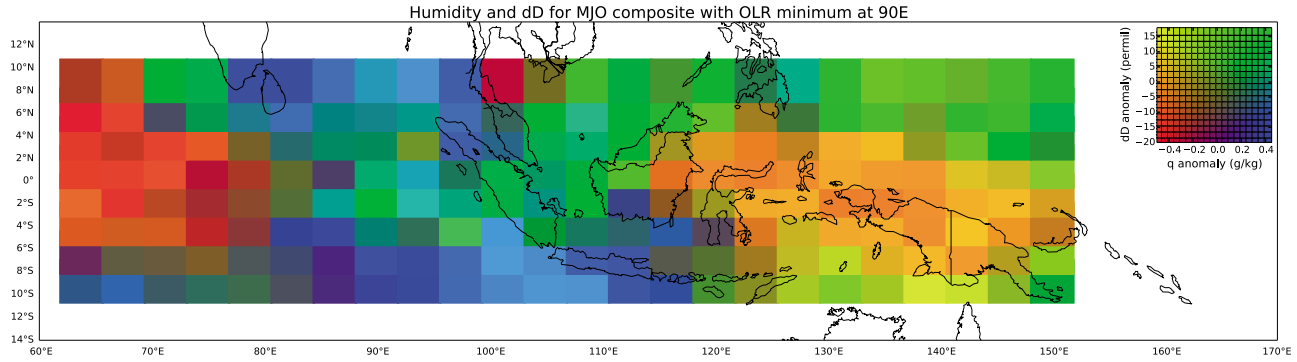

Figure 3. Composite of MJO events (2010–2012) with a peak of convective activity at 90°E; IASI ULB q and δD anomaly at 500 hPa. The inset shows the q-δD anomaly corresponding to the shading.

3. Results

This section presents the results of the current study in four parts. First, the available stable water isotope data sets are compared. Second, the composite mean IASI MJO q-δD phasing is described over all MJO events between March 2010 and March 2012, as well as its spatial variability. Third, the variability in the q-δD phasing between the events is determined. Finally, the LMDZ model is used to suggest which processes cause the typical q-δD phasing.

3.1. Composite q-δD Phasing Observed by IASI

Figure 3 shows the IASI ULB spatial q-δD anomalies when the MJO convective peak is at 90°E. The eastern part of the domain (around 130°E) is drier than normal, while the δD anomaly is minimal. At 110°E, the air is more humid and more enriched than normal, while at the convective peak (90–100°E) it is more humid and more depleted. In the areas where the event has just passed (60–80°E), the air is drier and more depleted than normal.

This spatial signal at a given time translates into a temporal signal at a given location. In this paper, we present q-δD anomalies, as the composite mean q-δD values varies for different MJO events. The type of MJO q-δD cycle and the tendencies found in LMDZ were independent of these composite mean q-δD values. Figure 4 shows the average q-δD phasing at 80°E. The IASI q increases from 20 days before the center of the event and peaks close to the OLR minimum, within the 5 days before the MJO event. After the OLR minimum, the humidity decreases again until it reaches normal values about 10 days after the peak of the event. The δD shows a different evolution. During the 20 days before the center of the event, there is only a small enrichment. However, from just before the OLR minimum, there is a strong depletion, and a minimum in δD is reached between 5 and 10 days after the peak of the event. When plotted in q-δD space (Figure 2), the mean q-δD evolution follows a clockwise path with four distinct phases, first moistening, then depletion, then drying, and lastly enrichment.

To take into account the lack of vertical sensitivity of satellite measurements in the comparison of IASI/TES δD and q profiles with LMDZ output, the latter needs to be degraded to the vertical sensitivity of the retrieval. This is achieved by convolving LMDZ output with the sensitivity matrices (averaging kernel matrices) of the retrievals. This was done following the method detailed in *Risi et al.* [2012]. Depending on the strength of the constraint used in the retrieval, the convolution can lead to significant differences. To test the impact of the convolution of LMDZ outputs with the averaging kernels, composite of MJO q-δD phasing (over seven MJO events from 2010 to 2012), starting about 20 days before the OLR minimum and ending about 20 days thereafter, with and without convolution is shown in Figure 4. The IASI data show a more clockwise cycle than both convolved and nonconvolved LMDZ model. The effect of the convolution on the LMDZ q-δD phasing is relatively small. This gives some confidence that the IASI MJO q and δD phasing observed in this study are not caused by a smoothing effect.

3.2. Comparison of Data Sets and Processing Methods

For the period October–December 2011, we analyzed the q-δD signal from the two different IASI retrieval schemes. Figure 5 shows a comparison between the IASI data set (using the ULB and KIT retrieval schemes) and surface-based data sets for different periods and locations. Note that the two retrieval schemes are not alike,

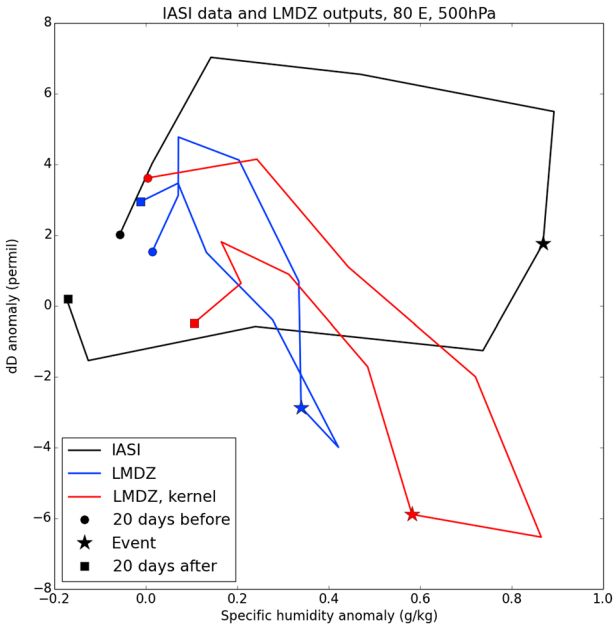

Figure 4. MJO cycles of q-δD anomalies at 500 hPa and 80°E for IASI ULB (composite mean over 2010–2012) for satellite data product, LMDZ, and convolved LMDZ. Cycles start 20 days before the MJO event (indicated with a circle symbol) and end 20 days after the center of the event (indicated with a box symbol). The MJO event is indicated with a star symbol.

because of differences in vertical sensitivities (smoothing) and in reliance on the prior. Therefore, retrieved δD and q values can differ in absolute values.

The ship-based measurements show higher q and δD anomalies than the IASI data sets during the MJO event, probably because the atmosphere is moister near the surface than in the midtroposphere. Due to the higher values of q and δD, as well as processes such as downdrafts and cold pools etc., the anomalies will also be higher at the surface than in the midtroposphere [*Yokoi et al.*, 2014]. Moreover, the IASI measurements are averages over a large area, which has a lower variability than the point measurement at the ship. It should also be noted that most of the MJO related convection was north of the equator during the CINDY/DYNAMO MJO events [*Johnson and Ciesielski*, 2013]. However, it is interesting to see that the clockwise q-δD phasing in

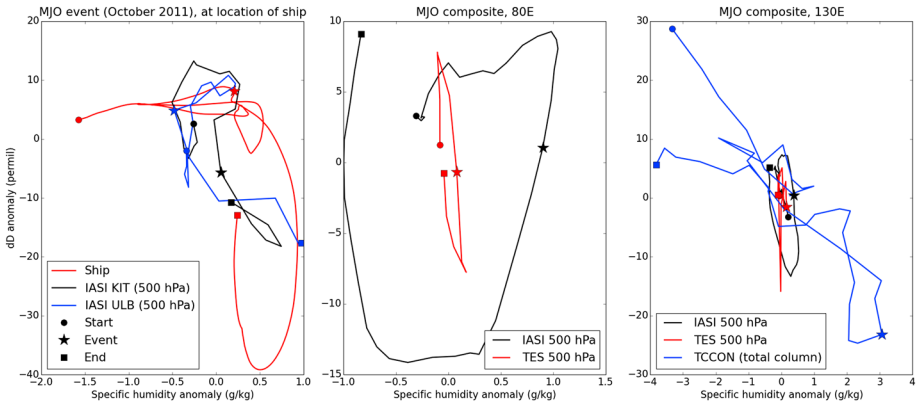

Figure 5. IASI q-δD measurements around for several MJO events. (left) Two q-δD retrieval algorithms (IASI KIT and IASI ULB) at 500 hPa compared to ship (surface) measurements taken during the CINDY/DYNAMO campaign. The IASI data are taken at the location of the ship (at about 80°E). Note that the time series stops 15 days after the MJO peak, because the ship was inoperationable at that time. (middle) Mean MJO at 80°E for IASI ULB (2010–2012) compared to TES (2006–2012). (right) TES (2006–2012) and IASI ULB (2010–2012) 500 hPa data at 130°E compared to TCCON total column data at Darwin, Australia (2004–2010).

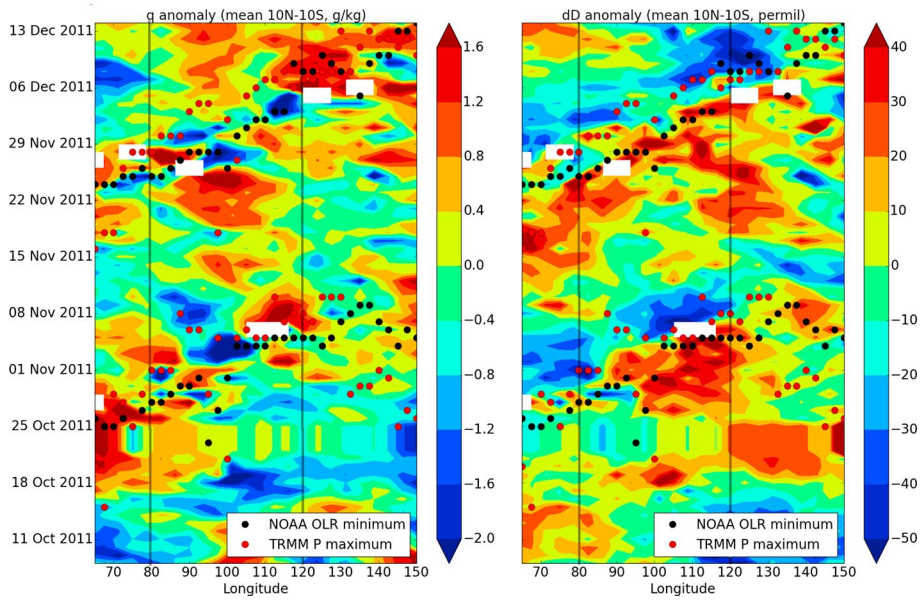

Figure 6. Hovmoller plot for IASI ULB q and δD anomalies at 500 hPa for October–December 2011. The NOAA OLR minimum and TRMM precipitation maximum are marked black and red. (Missing data due to cloud cover is indicated in white.)

the ship-based data is similar to the composite mean MJO signal from the IASI data, although this event does not show the clockwise phasing in the IASI data.

The comparison of the composite MJO event at 80°E from IASI data (mean over 2010–2012) to a composite of MJO events observed by TES (2006–2012) shows similar q-δD phasing (Figure 5b), although the IASI q amplitude is an order of magnitude larger than that observed by TES. At 120°E, over the maritime continent, the q-δD phasing is more anticorrelated in both IASI and TES data, which compares well with the TCCON total column measurements at Darwin, Australia. The amplitudes of the total column data are much larger than for the IASI data, which in turn has a somewhat larger q amplitude than the TES data.

Despite some differences in the q-dD signal in the different observational data sets, we feel sufficient confidence in the IASI retrievals to use the IASI data set to study spatial variability of the MJO, as well as variability across MJO events in the next sections.

3.3. Regional Differences in Composite MJO Signal

The MJO is a convectively coupled perturbation that moves eastward from the western side of the Indian Ocean basin into the Pacific, with a speed of about 5 m/s. However, physical processes and interactions may vary regionally and between MJO events.

During two MJO events (in October–December 2011) studied during CINDY/DYNAMO, interactions occurred on multiple scales between atmosphere and ocean, due to strong westerly wind bursts and a developing tropical cyclone [*Moum et al.*, 2014]. The moisture sources of the lower troposphere were different for the two MJO events, with low-frequency vertical transport drying the first MJO and moistening the second MJO [*Tseng et al.*, 2015]. The upward transport of this low-level moisture was caused by large-scale uplift and an absence of advection of midlevel dry air [*Hagos et al.*, 2014].

Figure 6 shows Hovmoller (time-longitude) plots for IASI ULB 500 hPa q and δD anomalies (averaged from 10°S to 10°N) for October–December 2011, during the CINDY/DYNAMO observation period. The CINDY/DYNAMO period contained two large MJO events, for which the filtered OLR minimum and the precipitation maximum are indicated. The specific humidity maximum coincides with the OLR minimum, whereas the δD minimum occurs about 10 days later. The q anomaly propagates eastward over the Indian Ocean (until 90°E) undisturbed. Farther east (over the maritime continent), the propagation is interrupted and negative humidity anomalies are present at the moment of the OLR minimum. In contrast, the δD signal propagates eastward over the maritime continent without interruption.

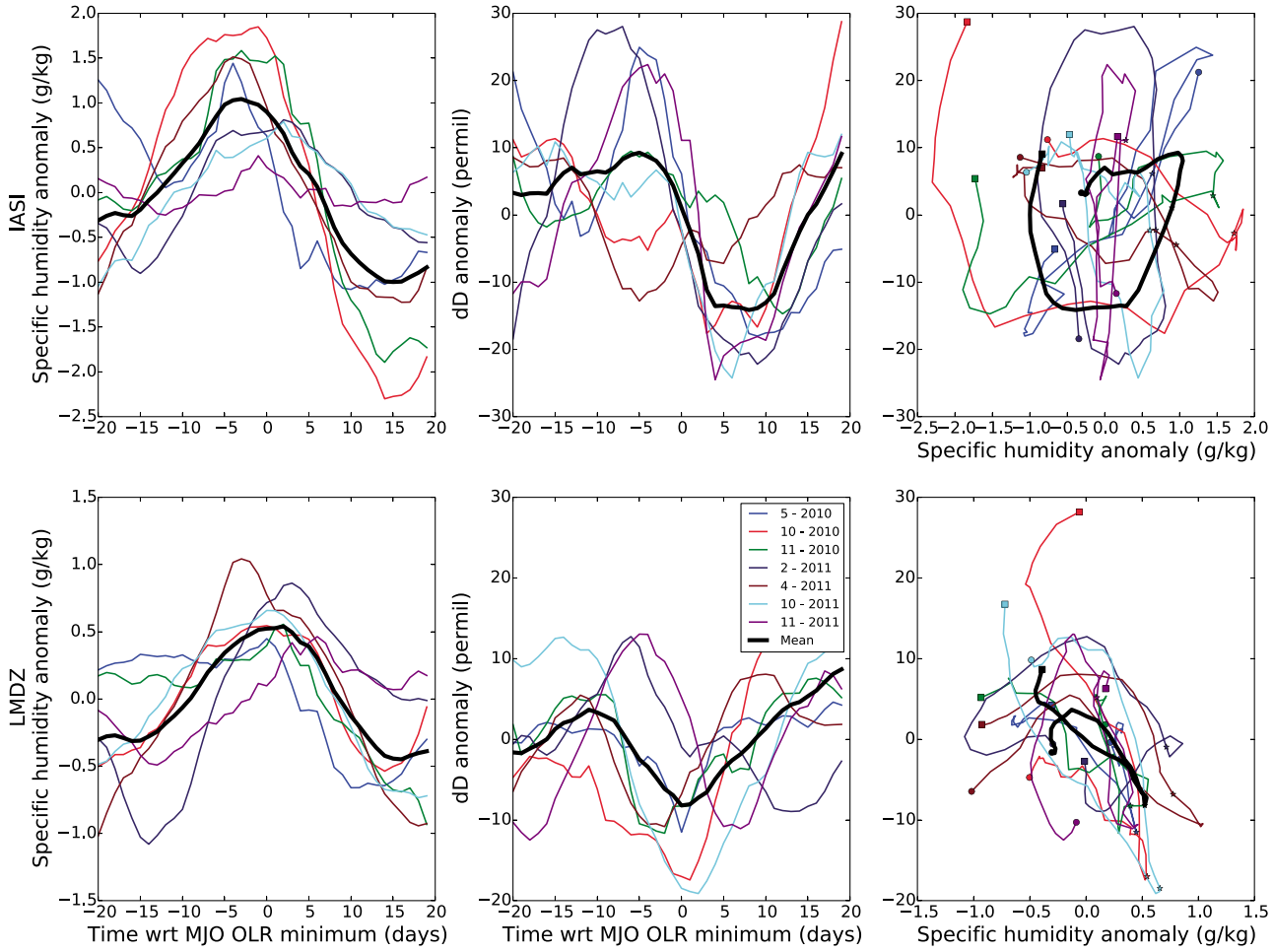

Figure 7. (left column) Humidity, (middle column) δD, and (right column) humidity versus δD evolution anomalies for MJO events in the Indian Ocean (80°E), for (top row) IASI ULB data and (bottom row) LMDZ GCM. The black curve shows the mean over all events.

From Figure 6, there appears to be a difference in temporal MJO q-δD evolution between the Indian Ocean and the maritime continent. Figure 7 shows the q-δD evolution (mean over 10°S–10°N) for all the events between March 2010 and March 2012 for the Indian Ocean (80°E) as measured by IASI (top row) and simulated by LMDZ (bottom row). Figure 8 shows the same for the maritime continent (120°E).

Over the Indian Ocean, the mean q-δD evolution follows a clockwise path with four distinct phases; first moistening, then depletion, then drying, and lastly enrichment. In contrast, over the maritime continent (Figure 8), the mean q-δD phasing is different, which is mostly due to a difference in humidity. The humidity peaks later than over the Indian Ocean, about 5 days after the MJO event. Moreover, the magnitude of the humidity anomaly is smaller over the maritime continent (about 0.5 g/kg) than over the Indian Ocean (about 1 g/kg). The evolution of δD anomalies is similar for the two regions, but again the mean anomalies over the Indian Ocean (about 15‰) are twice as big as over the maritime continent (about 8‰). Plotted in q-δD space, the mean MJO phasing follows a more anticorrelated pattern over the maritime continent, the atmosphere gets wetter and more depleted simultaneously, followed by drying and enrichment.

Figure 9 shows the spatial differences in composite mean humidity and δD MJO cycles. For this Figure, the amplitude and phasing of a mean MJO event was determined for each location by fitting a sinusoidal function (see section 2.5) through all q-δD observations relative to the MJO peak, defined as the OLR minimum. The first two panels depict the humidity maximum with respect to the MJO peak and the humidity amplitude, respectively. Over the Indian Ocean, there is not much spatial variability in the timing of this humidity maximum, which is just before the MJO peak. The humidity amplitude associated with the MJO is about 1 g/kg over the Indian Ocean. From 100°E to 120°E, the amplitude of the humidity anomaly is small (less than 0.3 g/kg).

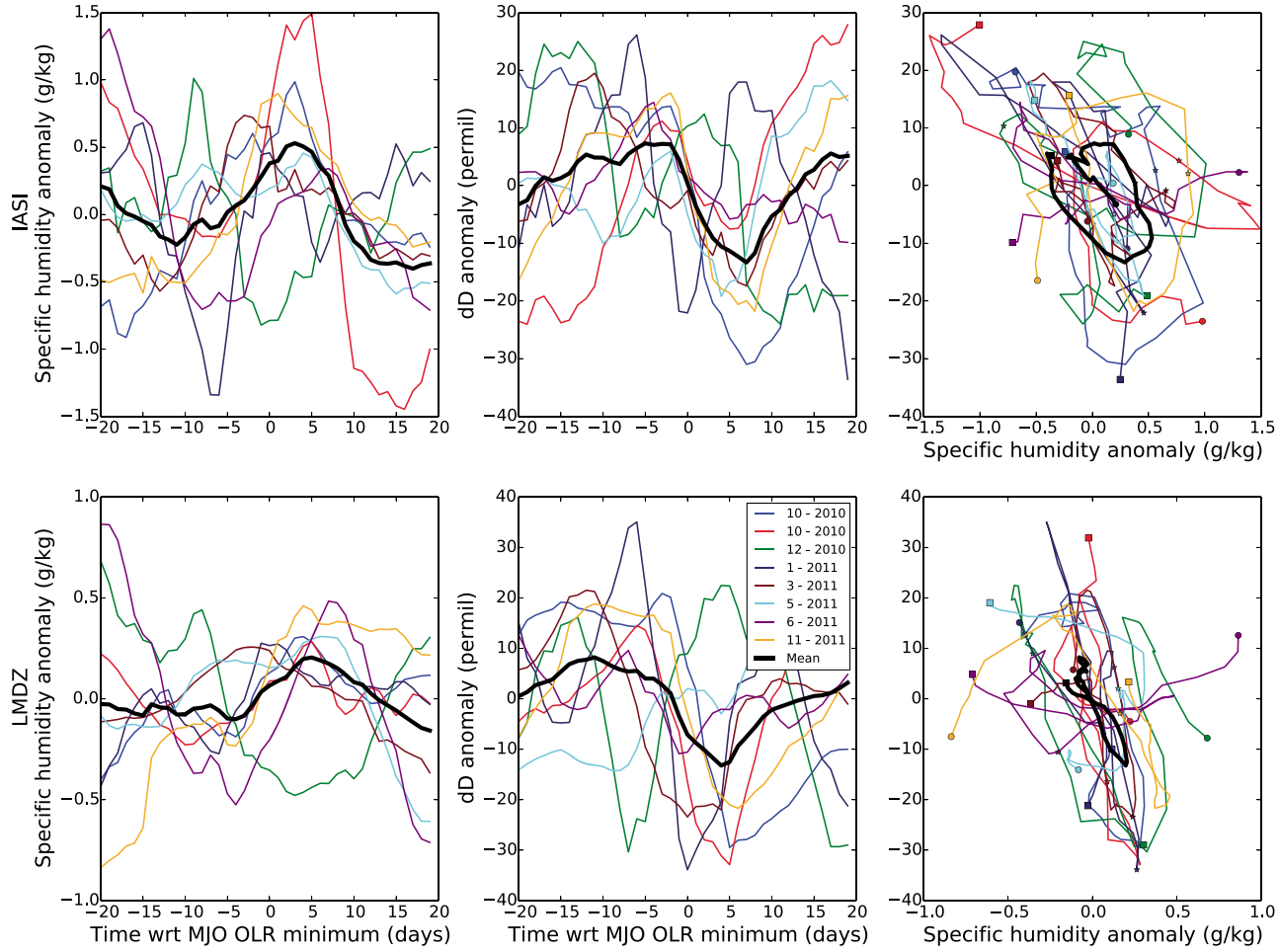

Figure 8. As in Figure 7 but for MJO events over the maritime continent (120°E). Note that the scales are different from those in Figure 7.

Therefore, variability on smaller time scales (like synoptic events) can be relatively more important for the humidity evolution and thus could explain why location of the maximum has a large spatial variability. Eastward of 120°E, the humidity maximum occurs a couple of days after the MJO peak, with a humidity amplitude of about 0.6 g/kg.

Figure 9 (third and fourth panels) depicts the same, only now for the δD evolution. Over the Indian Ocean, west of 90°E, the δD minimum consistently occurs about 10 days after the MJO peak, with an amplitude larger than 10‰. Between 90°E and 110°E, the δD amplitude decreases and the δD minimum occurs a somewhat later, 15 days after the peak of the event (although it is hard to diagnose the minimum, when the amplitude is small). Farther east over the maritime continent, between 110°E and 130°E, the amplitude increases again to about 10‰, while the minimum δD occurs at a similar moment as over the Indian Ocean, about 10 days after the peak of the event.

Figure 9 (fifth panel) shows the type of q-δD phasing (as plotted in Figures 7 and 8 (right columns) and as defined in section 2.5). Over the Indian Ocean, the mean q-δD phasing is either clockwise or correlated. Over the maritime continent, there are also areas where the mean phasing is anticorrelated, but there is no dominant mode.

The diagnosis of a mean signal over several MJO events is useful when the events are similar. Over the Indian Ocean, this is the case (see Figure 7), all events have a humidity peak and δD minimum at about the same time with respect to the MJO event peak, except for the April 2011 event, which has a q-δD cycle very unlike the other events. However, over the maritime continent, the q-δD phasing is different for different MJO events. The next section will discuss the variability between events.

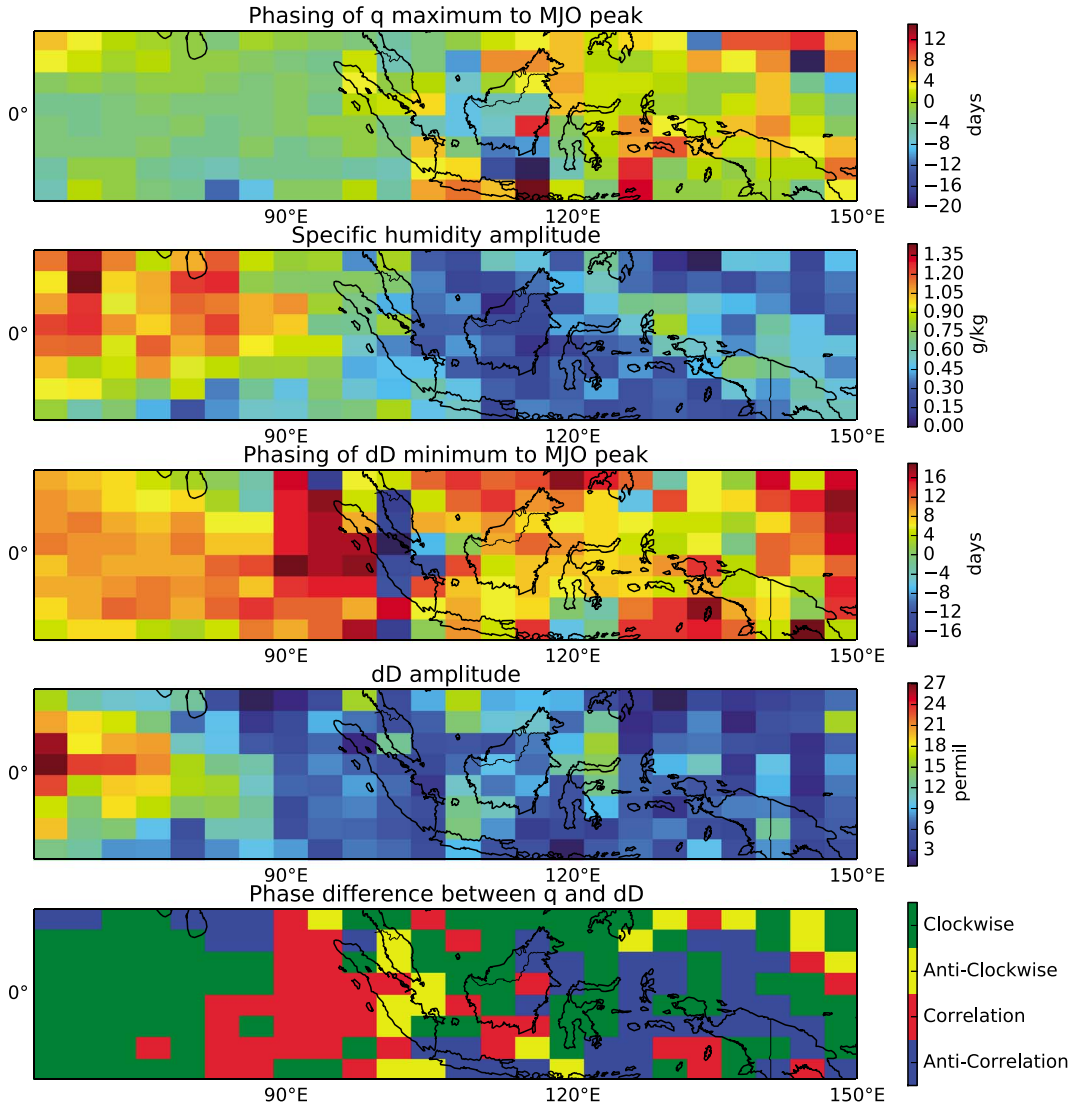

Figure 9. Spatial distribution in composite mean MJO q-δD cycles over the MJO domain, as observed by IASI ULB. (first panel) Differences between the q maximum and the MJO peak (negative values mean the q maximum is before the MJO peak) and (second panel) MJO q amplitude. Similar MJO (third panel) phasing and (fourth panel) amplitude for δD. (fifth panel) Type of q-δD phasing (clockwise, anticlockwise, correlated, or anticorrelated, see section 2.5).

3.4. Interevent Variability of MJO Signal

The composite IASI ULB MJO q-δD signal presented in section 3.3 shows that MJO events have different q-δD phasing over the Indian Ocean than over the maritime continent. However, the mean phasing plotted in Figure 9 (fifth panel) is a function of the mean q and δD phasing. This composite mean may not be a good measure to represent the dominant q-δD phasing as different phasings cancel out, which could mean that the mean phasing is not representative of the typical MJO event.

Over the Indian Ocean, most events resemble the mean (Figure 7). Only the events of May 2010 (correlated) and April 2011 (anticorrelated) have quite different phasing. The humidity evolution of all events is quite similar, with a peak in the 5 days before the center of the event and an amplitude between 0.5 and 1.5 g/kg. The δD evolution has some more variability between the events, especially for the two anomalous events. Almost all events have a minimal δD around 5 to 10 days after the MJO event, with an anomaly of around 20‰. In the 10 days before the OLR minimum, there is quite some δD variability between the events. Some events have a positive anomaly, while other events have a constant δD.

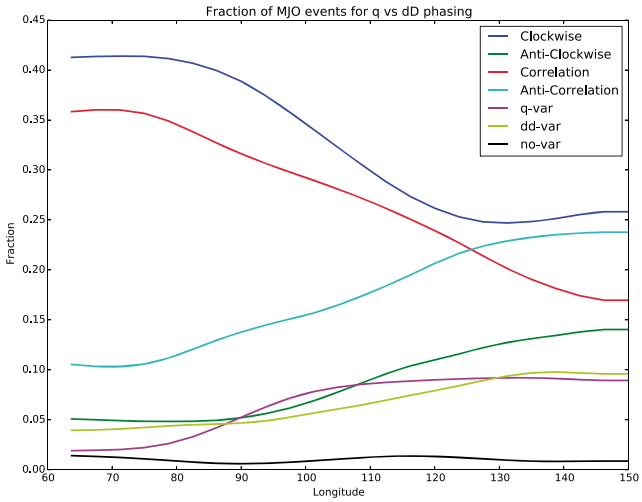

Figure 10. Longitudinal variation of fraction of type of q-δD phasing for MJO events, as observed by IASI ULB. If q amplitude is smaller than 0.1 g/kg, an event is classified as dd-var. If the δD amplitude is smaller than 5‰, an event is classified as q-var. If both q and δD amplitudes are below these thresholds, an event is classified as no-var.

Over the maritime continent at 120°E, the mean of the events is less representative of the individual events than over the Indian Ocean. The humidity peak varies across the events from 5 days before the center of the event to 5 days after the center of the event, while the humidity anomaly is generally smaller than 1 g/kg (with one event with a 1.5 g/kg anomaly). The δD phasing at 120°E varies a lot from event to event as well. Most events have decreasing δD from about 2 days before the center of the event following in a maximum depletion between 5 and 10 days after the center of the event. But the anomaly varies a lot across the events. Possible reasons for this variability across the events over the maritime continent are the strong diurnal cycle in convection due to diurnal heating over land, which competes with the MJO for moisture and energy, interference of topography with low-level moisture convergence, and a reduction of surface evaporation over land [*Zhang*, 2005; *Salby and Hendon*, 1994; *Wang and Li*, 1994; *Zhang*, 1997; *Maloney and Sobel*, 2004].

Over the Indian Ocean, the MJO events q-δD phasing is similar from event to event, while the events vary a lot over the maritime continent. Moreover, over the Indian Ocean, q and δD vary on the MJO intraseasonal time scale, while over the maritime continent, there is a lot more variability on the shorter synoptic time scales.

As mentioned at the start of this subsection, different q-δD phasings could cancel each other in the mean. To assess this, Figure 10 shows the fraction of type of MJO q-δD phasing (one of clockwise, anticlockwise, correlation, and anticorrelation) per longitude. For this Figure, for each longitude, all q-δD time series for the grid cells between 10°S and 10°N were analyzed separately, so the total number of events is the number of (LMDZ) grid cells between 10°S and 10°N (7) times the number of MJO events at that longitude (7 or 8, depending on the longitude). Over the Indian Ocean, from 70°E to 100°E, over two thirds of the events are either clockwise or correlated. Between 100°E and 120°E, the fraction of correlated events decreases, while the fraction of anticorrelated events increases to about 0.3. Eastward of 120°E, most events are either clockwise or anticorrelated.

3.5. Physical Interpretation of MJO Signal

This section presents a physical interpretation of the observed q-δD phasing. As shown in the previous sections, the typical MJO signal over the Indian Ocean is clockwise, while some events are more anticorrelated. Over the maritime continent, the events are generally more anticorrelated. We interpret the physical differences between clockwise and anticorrelated MJO event by analyzing the physical tendencies in the LMDZ atmospheric model for MJO events with similar q-δD phasing. With the large-scale dynamics nudged, LMDZ simulates a clockwise mean q-δD cycle as is observed in IASI; however, in LMDZ the drying and enrichment seem to occur more simultaneous than in the measurements. The LMDZ humidity amplitude is about half of that observed in IASI (Figure 4). In order to compare the physical processes of different types of MJO events, we selected MJO events that have a similar q-δD cycle in both the model and data. However, LMDZ is a GCM that does not simulate the MJO very well in free simulations, so the model may lack physical processes that are essential to the MJO.

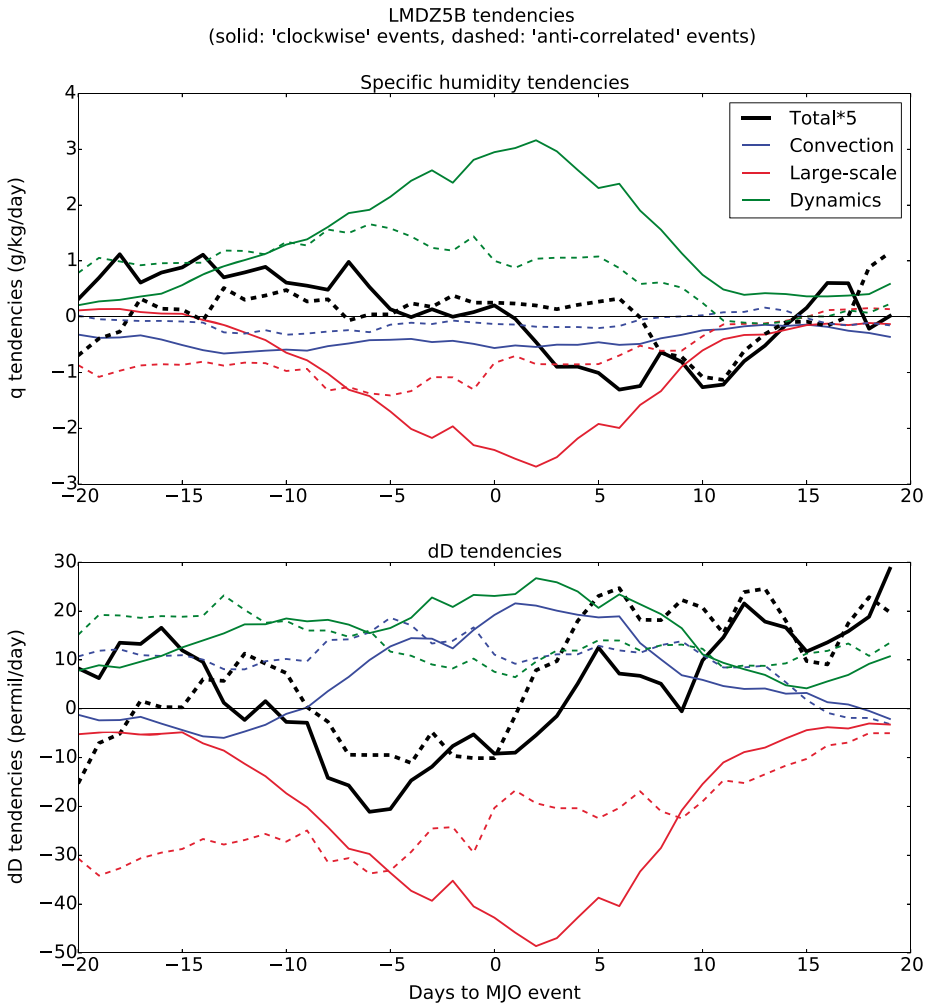

Figure 11. Five-day running mean of LMDZ tendencies at 80°E, 500 hPa for well-simulated clockwise and anticorrelated events. Boundary layer tendencies are negligible at 500 hPa and not shown.

Figure 11 shows the mean LMDZ tendencies at 500 hPa during the different MJO phases of clockwise events (February 2011 and October 2011, solid) and anticorrelated event (April 2011, dashed). In the midtroposphere (500 hPa), changes in the q-δD state are determined (in the LMDZ model) by convective, large-scale condensation, and advection tendencies. These tendencies are plotted in Figure 11, as well as the total tendency. Most of the time, the individual convective, large-scale condensation, and advection tendencies almost cancel out, resulting in a total tendency that is much smaller than the absolute value of its components.

From 20 to 10 days before the OLR minimum, there are small positive tendencies for both q and δD for both types of MJO events. The convective and large-scale condensation tendencies are small, the small moistening and enriching tendencies are due to the large-scale advection. This advection is dominated by vertical advection that brings water vapor from the boundary layer. The question of what moistens the boundary layer remains. The model is likely to fail to represent the moistening by congestus. So vertical advection in the model may represent a mixture of large-scale advection and cumulus congestus in nature.

During the 10 days before the OLR minimum, there is no large difference between the two types of MJO events. The advection tendencies increase; and more humid and enriched air is advected. There is a strong increase in large-scale condensation, which dries and depletes the atmosphere. These large-scale condensation tendencies almost balance the humidity advection, resulting in a small net wetting. The large-scale condensation depleting tendencies are larger than the large-scale dynamics enrichment, resulting in a net depletion during this period. The fact that the net convective humidity tendency is small does not imply that convection is not active. Detrainment may compensate for compensating subsidence drying, which are both

parts of the convection scheme. So during the 10 days before the OLR minimum, the model represents an atmosphere that is moistened by advection and moderately depleted by condensation in early MJO clouds.

In the 10 day period after the center of the event, there is a difference between the clockwise and anticorrelated MJO events. In the clockwise events, there is a net drying due to strongly drying large-scale condensation and some convective drying, which cannot be balanced by advection. The δD tendencies are close to zero, the strongly depleting large-scale condensation is compensated by and enrichment due to convection and advection. In contrast, in the anticorrelated event the humidity tendencies are balanced. The large-scale condensation dries less than in the clockwise case and is balanced by moistening due to advection. However, in the anticorrelated event, there is a strong net enrichment. The large-scale condensation depletes far less than in the clockwise events, as the convective and advection enrichment is similar to the clockwise events, there is net enrichment. As the large-scale condensation represents stratiform cloud types, the main difference between MJO events is the amount of stratiform clouds and precipitation 5–10 days after the OLR minimum.

During the period from 10 to 20 days after the center of the event, the convective and large-scale condensation tendencies decrease rapidly. The advection tendencies bring the q-δD state back to the initial state. These advection tendencies are also much smaller than during the peak of the MJO activity.

The main difference between the clockwise and anticorrelated MJO events in the LMDZ model (at 500 hPa) therefore seems to be the amount of large-scale condensation during the days after the OLR minimum. This large-scale condensation in the model is dependent on a humidity threshold for condensation, based on an assumed q distribution within the grid cell. Therefore, it may represent both stratiform or convective cloud processes in nature, but it is probably more representative for the stratiform clouds than the convective parameterization. This suggests that variability between the MJO events in the IASI q-δD observations might be related to the stratiform clouds in the 10 days after the MJO event.

4. Discussion

We now compare the outcomes of this study with other MJO studies using stable water isotopes and reflect on the use of these measurements for GCM evaluation.

Several previous studies have diagnosed the MJO using stable water isotopes measurements from other satellites, ground-based remote sensing, or in situ measurements. *Berkelhammer et al.* [2012] used data from the TES satellite [*Worden et al.*, 2006] (version 5) and found different q-δD phasing for a composite of MJO events from 2005 to 2009. Interestingly, the TES data showed anticlockwise q-δD phasing at 600 hPa over the maritime continent (90–120°E), which differs from the anticorrelated IASI data at 500 hPa over the maritime continent.

The TES satellite revisits the same location once every 2 weeks, while IASI has two measurements every day for each location. This means that for TES, only MJO composites can be made, while for IASI, the q-δD phasing for individual events can be determined. Given the variability between MJO events over the maritime continent, it is quite likely that the difference in the q-δD signal between TES and IASI is caused by different sampling of the MJO events, the TES phasing could be caused by a small number of outlier events. This would mean that difference in signal is probably not significant when taking into account the variability between events (Figure 8) [*Berkelhammer et al.*, 2012, Figure 7]. Alternatively, the difference in q-δD signal could originate from the different altitudes at which the signal was taken, which was 600 hPa for *Berkelhammer et al.* [2012] and 500 hPa for the current study or different data periods considered (2005–2009 for the TES data in *Berkelhammer et al.* [2012], compared to 2006–2012 for the TES data in the current study).

Kurita et al. [2011] studied two MJO events during October to December 2006 using ship-based in situ measurements and TES satellite δD data over the Indian Ocean. They found strong depletion during the peak of the MJO events due to strong convection, with strongest depletion corresponding to a maximum in stratiform rainfall a couple of days after the center of the event. This q-δD phasing and physical interpretation are similar to the IASI data and LMDZ interpretation in this study.

Noone [2012] devised a theoretical framework to interpret q-δD signals and to identify the processes involved. Using this framework, moistening in the tropics (Western Pacific) was found to be dominated by the reevaporation of falling raindrops, which is in line with importance of rain reevaporation hypothesized by *Worden et al.* [2007]. *Kurita et al.* [2011] found a large difference in the humidity and δD profile between convective

and stratiform precipitation and concluded that the δD measurements are suitable to detect the ratio of convective to stratiform precipitation. This is in line with the current study, as the main q-δD variability between MJO events is found in the ratio of stratiform large-scale and convective precipitation. As reevaporation occurs more during stratiform precipitation than during convective precipitation, this is also in line with the framework of *Noone* [2012]. A caveat is that reevaporation occurs mostly at lower levels, but it could deplete the lower atmosphere and be transported upward by convection and mesoscale circulations.

The interpretation of the MJO q-δD data is done using the nudged version of the LMDZ model. It is assumed that the model simulates the MJO processes in nature well, given the actual wind fields. In the IASI data, different q-δD cycles are found for different geographical locations and for different MJO events. These different cycles are also found in the model, in which each kind of cycle is associated with a specific sequence of events. When the q-δD phasing is clockwise, the large-scale condensation is maintained longer than when the q-δD phasing is anticorrelated.

The analysis presented in this study shows that the q-δD cycles can be used to determine the sequence of processes during the MJO and to assess whether the model is simulating this sequence correctly. In the current version of the LMDZ model, the q-δD cycles are anticorrelated too often. This suggests that large-scale condensation is not maintained long enough. Assuming that the large-scale condensation parameterization should represent a higher proportion of stratiform to convective clouds than convection parameterization, this suggests that LMDZ has difficulties simulating the stratiform clouds at the end of MJO events.

5. Conclusions

This research uses a satellite data set of midtropospheric joint measurements of a stable water isotope (δD) and specific humidity (q), applied to the tropical MJO domain for 2010–2012, including eight MJO events. In comparison with previous stable water isotope data sets [*Berkelhammer et al.*, 2012], a different mean MJO q-δD phasing is found. The current data set has a higher temporal resolution, which makes it possible to study individual MJO events.

The midtropospheric composite mean MJO q-δD signal has significant spatial variability. Over the Indian Ocean, MJO events follow a more clockwise pattern (in q-δD space). First, about 15 days before the peak of the MJO event, the atmosphere is moistened due to vertical advection. This causes only slight enrichment (larger δD values). Then, during the 10 days before the MJO event, large-scale condensation causes depletion, while humidity stays high. In the days after the center of the event, the air will remain depleted due to rain reevaporation from large-scale precipitation, while the air is drying. Finally, advection of dry enriched air will bring the q-δD values back to initial values.

In contrast, over the maritime continent, MJO events have a more anticorrelated pattern. The difference with the MJO sequence over the Indian Ocean is that during the days after the peak of the MJO event, there is less large-scale precipitation, possibly related to the presence of islands and a larger diurnal cycle. This causes the humidity to decrease and the δD to increase simultaneously between 5 and 15 days after the center of the event.

The variability in the 500 hPa q-δD signal between the events is small over the Indian Ocean, many events have a signal similar to the composite mean. However, there are some events that are more anticorrelated. The main interevent variability occurs during the 10 days after the event (OLR minimum). This variability is associated with different fractions of large scale to convective precipitation during that period.

Over the maritime continent, the interevent variability is much larger. There, there is much more variability in the q-δD signal on the synoptic time scale. Convection is not concentrated during the active phase of the MJO, as it is over the Indian Ocean. Thus, MJO q-δD signals are dominated by a signal on a shorter time scale.

The q-δD cycles simulated by models could serve as a basis to evaluate whether the convective parameterization and large-scale condensation are taking their correct role in dissipating the atmospheric instability. This could be used as a process-oriented diagnostic. For the LMDZ model, the q-δD cycles found will be used as a process-oriented diagnostic for comparison against sensitivity tests of parameters in the convective and large-scale condensations schemes.

Acknowledgments
All data for this paper are properly cited and referred to in the reference list. The GCM (LMDZ) simulations and tendencies are available from the authors upon request. The KIT IASI retrievals are made in the framework of the project MUSICA, which is funded by the European Research Council under the European Community's Seventh Framework Programme (FP7/2007-2013)/ERC grant agreement 256961. Part of this research was carried out at the Jet Propulsion Laboratory, California Institute of Technology, under a contract with the National Aeronautics and Space Administration. LMDZ simulations were performed at IDRIS under the allocation 0292 by GENCI. The authors thank the Editor and reviewers for their suggestions to improve the manuscript.

References

Benedict, J. J., and D. A. Randall (2007), Observed characteristics of the MJO relative to maximum rainfall, *J. Atmos. Sci.*, *64*(7), 2332–2354.
Berkelhammer, M., C. Risi, N. Kurita, and D. Noone (2012), The moisture source sequence for the Madden-Julian Oscillation as derived from satellite retrievals of HDO and H_2O, *J. Geophys. Res.*, *117*, D03106, doi:10.1029/2011JD016803.
Clerbaux, C., et al. (2009), Monitoring of atmospheric composition using the thermal infrared IASI/METOP sounder, *Atmos. Chem. Phys.*, *9*(16), 6041–6054.
Dee, D., et al. (2011), The ERA-interim reanalysis: Configuration and performance of the data assimilation system, *Q. J. R. Meteorol. Soc.*, *137*(656), 553–597.
Deutscher, N., et al. (2010), Total column CO_2 measurements at Darwin, Australia — Site description and calibration against in situ aircraft profiles, *Atmos. Meas. Tech.*, *3*(4), 947–958.
Dyroff, C., S. Sanati, E. Christner, A. Zahn, M. Balzer, H. Bouquet, J. B. McManus, Y. González-Ramos, and M. Schneider (2015), Airborne in situ vertical profiling of HDO/$H_2^{16}O$ in the subtropical troposphere during the MUSICA remote sensing validation campaign, *Atmos. Meas. Tech. Discuss.*, *8*(1), 121–155, doi:10.5194/amtd-8-121-2015.
Flatau, M., P. J. Flatau, P. Phoebus, and P. P. Niiler (1997), The feedback between equatorial convection and local radiative and evaporative processes: The implications for intraseasonal oscillations, *J. Atmos. Sci.*, *54*(19), 2373–2386.
Galewsky, J., and J. V. Hurley (2010), An advection-condensation model for subtropical water vapor isotopic ratios, *J. Geophys. Res.*, *115*, D16116, doi:10.1029/2009JD013651.
Hagos, S., Z. Feng, K. Landu, and C. N. Long (2014), Advection, moistening, and shallow-to-deep convection transitions during the initiation and propagation of Madden-Julian Oscillation, *J. Adv. Model. Earth Syst.*, *6*, 938–949, doi:10.1002/2014MS000335.
Huffman, G. J., D. T. Bolvin, E. J. Nelkin, D. B. Wolff, R. F. Adler, G. Gu, Y. Hong, K. P. Bowman, and E. F. Stocker (2007), The TRMM multisatellite precipitation analysis (TMPA): Quasi-global, multiyear, combined-sensor precipitation estimates at fine scales, *J. Hydrometeorol.*, *8*(1), 38–55.
Hung, M.-P., J.-L. Lin, W. Wang, D. Kim, T. Shinoda, and S. J. Weaver (2013), MJO and convectively coupled equatorial waves simulated by CMIP5 climate models, *J. Clim.*, *26*(17), 6185–6214.
Johnson, R. H., and P. E. Ciesielski (2013), Structure and properties of Madden-Julian Oscillations deduced from dynamo sounding arrays, *J. Atmos. Sci.*, *70*(10), 3157–3179.
Kiladis, G. N., and K. M. Weickmann (1992), Circulation anomalies associated with tropical convection during northern winter, *Mon. Weather Rev.*, *120*(9), 1900–1923.
Kim, D., et al. (2009), Application of MJO simulation diagnostics to climate models, *J. Clim.*, *22*(23), 6413–6436.
Kim, D., A. H. Sobel, A. D. Del Genio, Y. Chen, S. J. Camargo, M.-S. Yao, M. Kelley, and L. Nazarenko (2012), The tropical subseasonal variability simulated in the NASA GISS general circulation model, *J. Clim.*, *25*(13), 4641–4659.
Kurita, N., D. Noone, C. Risi, G. A. Schmidt, H. Yamada, and K. Yoneyama (2011), Intraseasonal isotopic variation associated with the Madden-Julian Oscillation, *J. Geophys. Res.*, *116*, D24101, doi:10.1029/2010JD015209.
Lacour, J.-L., C. Risi, L. Clarisse, S. Bony, D. Hurtmans, C. Clerbaux, and P.-F. Coheur (2012), Mid-tropospheric δd observations from IASI/METOP at high spatial and temporal resolution, *Atmos. Chem. Phys.*, *12*(22), 10,817–10,832, doi:10.5194/acp-12-10817-2012.
Lacour, J.-L., L. Clarisse, J. Worden, M. Schneider, S. Barthlott, F. Hase, C. Risi, C. Clerbaux, D. Hurtmans, and P.-F. Coheur (2015), Cross-validation of IASI/METOP derived tropospheric δd with TES and ground-based FTIR observations, *Atmos. Meas. Tech.*, *8*(3), 1447–1466.
Lau, K., and L. Peng (1987), Origin of low-frequency (intraseasonal) oscillations in the tropical atmosphere. Part I: Basic theory, *J. Atmos. Sci.*, *44*(6), 950–972.
Liebmann, B., and C. Smith (1996), Description of a complete (interpolated) outgoing longwave radiation dataset, *Bull. Am. Meteorol. Soc.*, *77*(6), 1275–1277.
Madden, R. A., and P. R. Julian (1972), Description of global-scale circulation cells in the tropics with a 40–50 day period, *J. Atmos. Sci.*, *29*(6), 1109–1123.
Maloney, E. D., and D. L. Hartmann (2001), The sensitivity of intraseasonal variability in the NCAR CCM3 to changes in convective parameterization, *J. Clim.*, *14*(9), 2015–2034.
Maloney, E. D., and A. H. Sobel (2004), Surface fluxes and ocean coupling in the tropical intraseasonal oscillation, *J. Clim.*, *17*(22), 4368–4386.
Matthews, A. J. (2000), Propagation mechanisms for the Madden-Julian Oscillation, *Q. J. R. Meteorol. Soc.*, *126*(569), 2637–2651.
Moum, J. N., et al. (2014), Air-sea interactions from westerly wind bursts during the November 2011 MJO in the Indian Ocean, *Bull. Am. Meteorol. Soc.*, *95*(8), 1185–1199.
Noone, D. (2012), Pairing measurements of the water vapor isotope ratio with humidity to deduce atmospheric moistening and dehydration in the tropical midtroposphere, *J. Clim.*, *25*(13), 4476–4494.
Randall, D. A. (2013), Beyond deadlock, *Geophys. Res. Lett.*, *40*, 5970–5976, doi:10.1002/2013GL057998.
Rio, C., F. Hourdin, J.-Y. Grandpeix, and J.-P. Lafore (2009), Shifting the diurnal cycle of parameterized deep convection over land, *Geophys. Res. Lett.*, *36*, L07809, doi:10.1029/2008GL036779.
Risi, C., S. Bony, F. Vimeux, and J. Jouzel (2010), Water-stable isotopes in the LMDZ4 general circulation model: Model evaluation for present-day and past climates and applications to climatic interpretations of tropical isotopic records, *J. Geophys. Res.*, *115*, D12118, doi:10.1029/2009JD013255.
Risi, C., et al. (2012), Process-evaluation of tropospheric humidity simulated by general circulation models using water vapor isotopologues: 1. Comparison between models and observations, *J. Geophys. Res.*, *117*, D05303, doi:10.1029/2011JD016621.
Rokotyan, N., et al. (2014), A posteriori calculation of δ18O and δD in atmospheric water vapour from ground-based near-infrared FTIR retrievals of $H_2{}^{16}O$, $H_2{}^{18}O$, and $HD^{16}O$, *Atmos. Meas. Tech.*, *7*(8), 2567–2580.
Salby, M. L., and H. H. Hendon (1994), Intraseasonal behavior of clouds, temperature, and motion in the tropics, *J. Atmos. Sci.*, *51*(15), 2207–2224.
Schneider, M., and F. Hase (2011), Optimal estimation of tropospheric H_2O and δd with IASI/METOP, *Atmos. Chem. Phys.*, *11*(21), 11,207–11,220.
Schneider, M., et al. (2012), Ground-based remote sensing of tropospheric water vapour isotopologues within the project MUSICA, *Atmos. Meas. Tech.*, *5*(12), 3007–3027, doi:10.5194/amt-5-3007-2012.
Schneider, M., et al. (2015), Empirical validation and proof of added value of MUSICA's tropospheric d remote sensing products, *Atmos. Meas. Tech.*, *8*(1), 483–503, doi:10.5194/amt-8-483-2015.
Sobel, A., and E. Maloney (2013), Moisture modes and the eastward propagation of the MJO, *J. Atmos. Sci.*, *70*(1), 187–192.
Sobel, A., S. Wang, and D. Kim (2014), Moist static energy budget of the MJO during dynamo, *J. Atmos. Sci.*, *71*(11), 4276–4291.

Thayer-Calder, K., and D. A. Randall (2009), The role of convective moistening in the Madden-Julian Oscillation, *J. Atmos. Sci.*, *66*(11), 3297–3312.

Tseng, K.-C., C.-H. Sui, and T. Li (2015), Moistening processes for Madden-Julian Oscillations during DYNAMO/CINDY, *J. Clim.*, *28*(8), 3041–3057.

Wang, B., and T. Li (1994), Convective interaction with boundary-layer dynamics in the development of a tropical intraseasonal system, *J. Atmos. Sci.*, *51*(11), 1386–1400.

Wiegele, A., et al. (2014), The MUSICA METOP/IASI H_2O and δD products: Characterisation and long-term comparison to NDACC/FTIR data, *Atmos. Meas. Tech.*, *7*(8), 2719–2732, doi:10.5194/amt-7-2719-2014.

Woolnough, S., F. Vitart, and M. Balmaseda (2007), The role of the ocean in the Madden-Julian Oscillation: Implications for MJO prediction, *Q. J. R. Meteorol. Soc.*, *133*(622), 117–128.

Worden, J., et al. (2006), Tropospheric emission spectrometer observations of the tropospheric HDO/H_2O ratio: Estimation approach and characterization, *J. Geophys. Res.*, *111*, D16309, doi:10.1029/2005JD006606.

Worden, J., et al. (2007), Importance of rain evaporation and continental convection in the tropical water cycle, *Nature*, *445*(7127), 528–532.

Worden, J., S. Kulawik, C. Frankenberg, V. Payne, K. Bowman, K. Cady-Peirara, K. Wecht, J.-E. Lee, and D. Noone (2012), Profiles of CH_4, HDO, H_2O, and N_2O with improved lower tropospheric vertical resolution from Aura TES radiances, *Atmos. Meas. Tech.*, *5*(2), 397–411.

Yokoi, S., M. Katsumata, and K. Yoneyama (2014), Variability in surface meteorology and air-sea fluxes due to cumulus convective systems observed during CINDY/DYNAMO, *J. Geophys. Res. Atmos.*, *119*, 2064–2078, doi:10.1002/2013JD020621.

Zhang, C. (1997), Intraseasonal variability of the upper-ocean thermal structure observed at 0° and 165° e*, *J. Clim.*, *10*(12), 3077–3092.

Zhang, C. (2005), Madden-Julian Oscillation, *Rev. Geophys.*, *43*, RG2003, doi:10.1029/2004RG000158.

Zhang, C. (2013), Madden-Julian Oscillation: Bridging weather and climate, *Bull. Am. Meteorol. Soc.*, *94*(12), 1849–1870.

Zhang, C., J. Gottschalck, E. D. Maloney, M. W. Moncrieff, F. Vitart, D. E. Waliser, B. Wang, and M. C. Wheeler (2013), Cracking the MJO nut, *Geophys. Res. Lett.*, *40*, 1223–1230, doi:10.1002/grl.50244.